Inorganic Chemistry
Article
Cite This: Inorg. Chem. XXXX, XXX, XXX−XXX
pubs.acs.org/IC

Synthesis, Characterization, and Electrochemistry of the Homoleptic f Element Ketimide Complexes $[Li]_2[M(N{=}C^tBuPh)_6]$ (M = Ce, Th)

Mikiyas K. Assefa, Dumitru-Claudiu Sergentu, Lani A. Seaman, Guang Wu, Jochen Autschbach,* and Trevor W. Hayton*

Department of Chemistry and Biochemistry, University of California Santa Barbara, 93106 Santa Barbara, California, United States
Department of Chemistry, University at Buffalo, State University of New York, 14260 Buffalo, New York, United States

Supporting Information

ABSTRACT: Reaction of $[Ce(NO_3)_3(THF)_4]$ with 6 equiv of $Li(N{=}C^tBuPh)$, followed by addition of 0.5 equiv of I_2, affords the homoleptic Ce(IV) ketimide $[Li]_2[Ce(N{=}C^tBuPh)_6]$ (**1**), which can be isolated in 44% yield after workup. Similarly, reaction of $[ThCl_4(DME)_2]$ (DME = 1,2-dimethoxyethane) with 6 equiv of $Li(N{=}C^tBuPh)$ in tetrahydrofuran affords the isostructural Th(IV) ketimide $[Li]_2[Th(N{=}C^tBuPh)_6]$ (**2**), which can be isolated in 53% yield after workup. Both **1** and **2** were fully characterized, including analysis by X-ray crystallography, allowing for a detailed structural and spectroscopic comparison. The electronic structures of **1** and **2** were also explored with density functional theory and multiconfigurational wave function calculations. Additionally, the redox chemistry of **1** was probed by cyclic voltammetry, which revealed a highly cathodic Ce(IV)/Ce(III) reduction potential, providing evidence for the ability of the ketimide ligand to stabilize high oxidation states of the lanthanides.

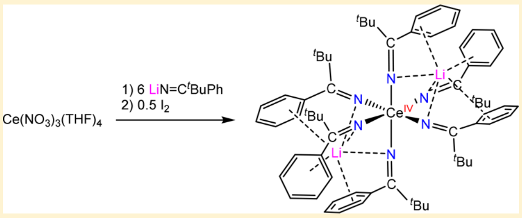

INTRODUCTION

The chemistry of high-valent lanthanide ions has remained enigmatic.[1−7] Indeed, cerium is the only lanthanide element that can easily form stable molecular +4 complexes, which has paved the way for extensive study of its redox properties, both in solid state and solution.[8−16] This redox chemistry is relevant to both fundamental and applied research.[17−33] For example, multiconfigurational ground states (GSs) have recently been revealed in several molecular and solid-state Ce(IV) materials.[25,29−37] Moreover, X-ray absorption spectroscopy and density functional theory (DFT) studies on tetravalent cerium have revealed considerable covalency and f orbital participation in Ce(IV)-L bonding.[24−29,38] In addition, the Ce(IV/III) redox couple has proved instrumental for separation of cerium from mineral ores and in the mechanism of action of several ceria-supported catalysts.[8,10,23,39,40] Despite these successes, there still are only a handful of ligands that are capable of stabilizing high oxidation states in the lanthanides, especially in nonaqueous environments. Examples include nitroxide,[9] tetraazaannulene,[41] imidophosphorane,[14,42] atrane,[16] binolate,[43] silyloxide,[44] and methanediide.[27,45,46]

The ketimide ligand ($R_2C{=}N^-$) is considered to be strongly electron donating and, thus, is predicted to stabilize high oxidation states in otherwise oxidizing metal centers. For example, our group has previously utilized this ligand to synthesize the tetravalent transition-metal ketimides $M(N{=}C^tBu_2)_4$ (M = Mn, Fe, Co, V, Nb, Ta) in moderate to good yields.[47−50] Similarly, Hoffman and co-workers have reported the synthesis of the analogous group VI ketimides $M(N{=}C^tBu_2)_4$ (M = Cr, Mo, W).[51] DFT calculations and ligand field analyses on these complexes have found that the ketimide ligand is a strong σ- and π-donor, as well as a strong π-acceptor.[47,48,51,52] Drawing on these results, we endeavored to probe the extent to which this ligand can stabilize high oxidation states in the lanthanides, specifically in cerium. While the synthesis and redox chemistry of high-valent actinide ketimides has recently been explored,[53−55] to our knowledge, that of the lanthanide analogues is unknown. Herein, we describe the synthesis and computational and electrochemical analysis of a homoleptic cerium(IV) ketimide and its isostructural thorium(IV) analogue.

RESULTS AND DISCUSSION

Synthesis and Characterization. Reaction of $[Ce(NO_3)_3(THF)_4]$ with 6 equiv of $Li(N{=}C^tBuPh)$, in tetrahydrofuran (THF), followed by addition of 0.5 equiv of I_2, results in the formation of a deep purple solution. Workup of this solution results in isolation of $[Li]_2[Ce(N{=}C^tBuPh)_6]$ (**1**), as purple plates in 44% yield (Scheme 1). Intriguingly, **1** is also formed in small quantities during the reaction of $Li(N{=}C^tBuPh)$ with $[Ce(NO_3)_3(THF)_4]$, in the absence of I_2, according to a ^1H NMR spectrum of an aliquot of the reaction mixture. The oxidation to Ce(IV) under these conditions can likely be attributed to the redox activity of the nitrate coligand in the $[Ce(NO_3)_3(THF)_4]$ starting material, which has been shown to oxidize Ce(III) under certain conditions.[56]

Complex **1** is readily soluble in diethyl ether (Et_2O), toluene, and THF, but only sparingly soluble in nonpolar aliphatic solvents, such as hexanes. Its IR spectrum exhibits two

Received: May 15, 2019

DOI: 10.1021/acs.inorgchem.9b01428
Inorg. Chem. XXXX, XXX, XXX−XXX

Scheme 1. Synthesis of Complexes 1 and 2

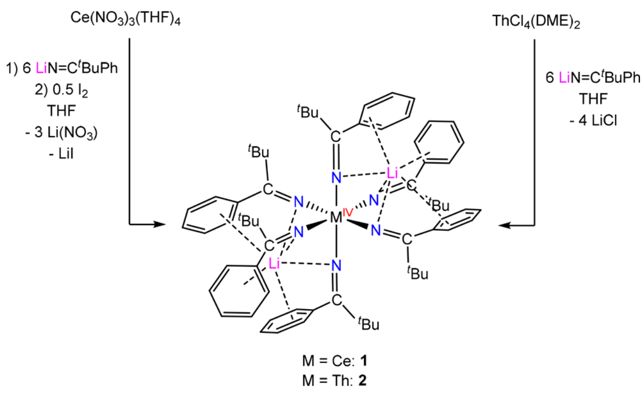

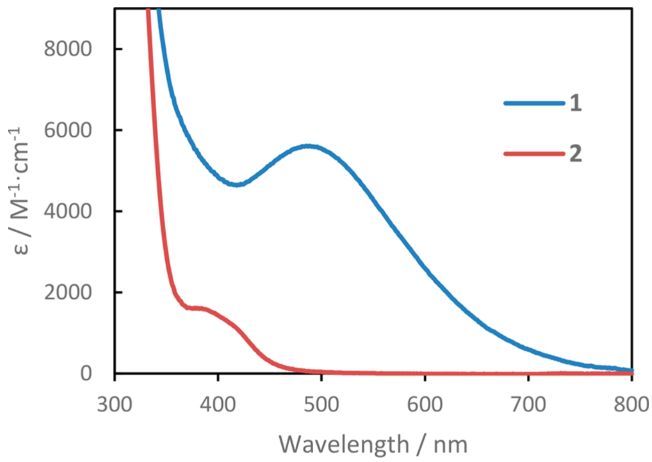

Figure 1. UV−Vis spectra of **1** (0.089 mM) and **2** (0.13 mM) in toluene.

strong absorptions at 1624 and 1637 cm^{-1} assignable to the C═N stretches of the ketimide ligand. Additionally, its ^1H NMR spectrum in C_6D_6 features a sharp singlet at 1.36 ppm, integrating to 54 protons, which is attributable to the *tert*-butyl protons of the ketimide ligand. This spectrum also features two multiplets at 6.62 and 6.99 ppm that integrate to 12 and 18 protons, respectively, which are assignable to the *ortho* and overlapping *meta*/*para* protons of the ketimide phenyl rings. The $^{13}C\{^1H\}$ NMR spectrum of **1** in C_6D_6 exhibits a resonance at 175.08 ppm assignable to the ketimide C═N environment. This chemical shift is nearly identical to that observed for the C═N resonance in the octahedral U(VI) ketimide complex [U(N═C^tBuPh)$_6$] (180.40 ppm).[55] Finally, the $^7Li\{^1H\}$ NMR spectrum of **1** in C_6D_6 features a single resonance at 0.06 ppm. Likewise, the $^7Li\{^1H\}$ NMR spectrum of **1** in toluene-d_8 features a single resonance at −0.02 ppm (Figure S5). Curiously, though, the $^7Li\{^1H\}$ NMR spectrum of **1** in THF-d_8 features broad resonances at 1.94, 1.75, and 0.65 ppm (Figure S7). The resonances at 1.94 and 1.75 ppm are assignable to free Li(N═C^tBuPh) (Figure S16),[57] suggesting that dissociation of 1 equiv of Li(N═C^tBuPh) from **1** occurs in this solvent, resulting in formation of [Li][Ce(N═C^tBuPh)$_5$] (**1′**). Consistent with this hypothesis, the $^7Li\{^1H\}$ signals assignable to Li(N═C^tBuPh) and **1′** are present in a 1:1 ratio. No evidence for the dissociation of Li(N═C^tBuPh) from **1** is observed in C_6D_6 or toluene-d_8, suggesting that the strong donor ability of THF facilitates formation of the lithium ketimide salt. Finally, complex **1** features moderate thermal stability: a solution of **1** in C_6D_6 exhibits ∼20% decomposition after 2 d at room temperature, according to ^1H NMR spectroscopy. The principal decomposition product appears to be a Ce(III) complex on the basis of the paramagnetically shifted resonances observed in the ^1H NMR spectrum.

The UV−vis spectrum of **1** in toluene exhibits a strong, broad absorption at 485 nm (ε = 5600 $M^{-1}\cdot cm^{-1}$), which is assignable to a ligand-to-metal charge transfer (Figure 1; also see discussion below). It is quite common for Ce(IV) complexes to be deeply colored. For example, [Ce(trop)$_4$][31] and [Ce(η^8-Pn*)$_2$][30] feature intense and broad LMCT absorptions at 450 and 530 nm, respectively. [Ce(cot)$_2$], [Ce(tmtaa)$_2$], and [Ce(BIPM^{TMS})$_2$] are also deeply colored.[34,58,59,46] We also measured the solid-state magnetic susceptibility of **1** using superconducting quantum interference device (SQUID) magnetometry. Significantly, this measurement reveals temperature-independent paramagnetism (TIP) for **1**. The value of χ_{TIP}, extracted from the temperature -dependent χT data (Figure S32), is 4.91 × 10^{-4} emu/mol, which is comparable to the χ_{TIP} values reported for Ce(tmtaa)$_2$ (2.33 × 10^{-4} emu/mol), Ce(cot)$_2$ (1.4 × 10^{-4} emu/mol), and Ce(acac)$_4$ (2.1 × 10^{-4} emu/mol).[31,35] The observation of TIP in Ce(IV) complexes has been interpreted as evidence of multiconfigurational character.[31] However, it could also simply indicate field-induced mixing of a closed-shell singlet ground state with a low-lying triplet excited state, as is known for some U(VI) complexes and d^0 transition-metal oxo anions.[60−62]

Crystals of **1** suitable for an X-ray diffraction analysis were grown from a dilute pentane solution stored at −25 °C. Complex **1** crystallizes in the rhombohedral space group $R\bar{3}$, and its solid-state molecular structure is shown in Figure 2. A selection of metrical parameters can be found in Table 1. In the solid state, **1** adopts a distorted octahedral geometry (e.g., N1−Ce1−N1* = 81.8(2)° and N1−Ce1−N1** = 98.2(2)°) about the Ce center, which is ligated by six crystallographically equivalent ketimide ligands. The C═N bond distance in **1** (1.256(8) Å) is similar to that observed in the U(V) ketimide, [Li][U(N═C^tBuPh)$_6$] (1.260(3) Å),[55] and other homoleptic transition metal ketimides (1.25−1.27 Å).[47−51] The Ce−N

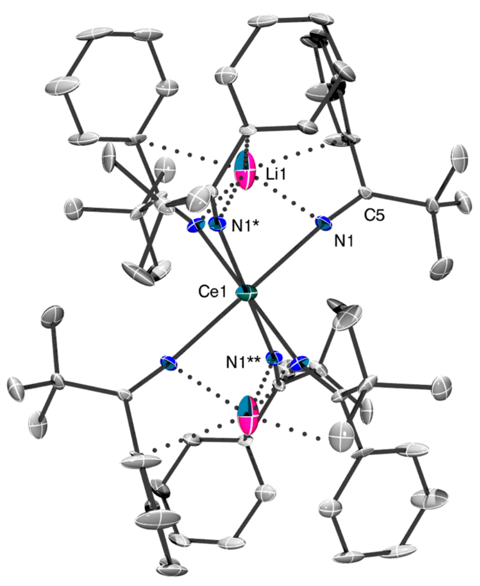

Figure 2. Solid-state molecular structure of **1**. Hydrogen atoms omitted for clarity.

DOI: 10.1021/acs.inorgchem.9b01428
Inorg. Chem. XXXX, XXX, XXX−XXX

Table 1. Selected Bond Lengths (Å) and Angles (deg) for Complexes 1 and 2

	1	2
M−N	2.338(5)	2.376(2)
C−N	1.256(8)	1.257(2)
Li1−N1	2.138(19)	2.166(4)
Li1−C_{ipso}	2.918(11)	2.908(2)
M−N1−C5	165.9(5)	166.24(14)
N1−M−N1*	81.8(2)	79.78(6)
N1−M−N1**	98.2(2)	100.22(6)

bond length (2.338(5) Å) is longer than those reported for the homoleptic Ce(IV) phosphoiminato complex [Ce(NP-$(pip)_3)_4$] (average (av) 2.20(2) Å),[14] and the Ce(IV) amides [Ce($N^iPr_2)_4$] (2.225(1) and 2.223(1) Å),[63] [Ce$(NCy_2)_4$] (2.238(5)−2.247(6) Å),[64] and [Ce(N$(SiHMe_2)_2)_4$] (2.2378(11)−2.2574(11) Å),[65] likely due to the higher coordination number in **1**, as well as the dianionic charge at the Ce center. This distance is also considerably longer than the U−N distance in the structurally similar U(V) ketimide complex [Li][U(N=C^{t}BuPh$)_6$] (2.217(2) Å),[55] consistent with the larger ionic radius of Ce(IV). The structure of **1** also features two Li cations within the secondary coordination sphere. These ions are supported by dative interactions with three nitrogen atoms and the ipso carbons of three phenyl rings. The Li−N distance (2.138(19) Å) is shorter than that in [Li][U(N=C^{t}BuPh$)_6$] (2.265(16) Å), which features a Li ion with an identical binding mode.[55] Finally, the Ce−N−C angle (165.9(5)°) is slightly smaller than the U−N−C angle in [Li][U(N=C^{t}BuPh$)_6$] (176.9(2)°),[55] which may be a consequence of the longer M−N bond lengths in **1**.

To better contextualize our cerium results, we sought to synthesize the analogous thorium(IV) ketimide complex $[Li]_2$[Th(N=C^{t}BuPh$)_6$] (**2**). Complex **2** was prepared by reaction of [$ThCl_4(DME)_2$] (DME = 1,2-dimethoxyethane) with 6 equiv of Li(N=C^{t}BuPh) in THF (Scheme 1). Workup of the reaction mixture followed by recrystallization from a concentrated THF/hexanes solution afforded **2** as yellow blocks in 53% yield. Curiously, reaction of UCl_4 with 6 equiv of Li(N=C^{t}BuPh) only resulted in formation of the 5-coordinate ketimide complex, [Li$(THF)_2$][U(N=C^{t}BuPh$)_5$], a difference that likely reflects the smaller ionic radius of U(IV).[55]

Complex **2** is soluble in Et_2O, toluene, and THF, but it features limited solubility in pentanes or hexanes. Its UV−vis spectrum in toluene is missing the obvious ligand-to-metal charge transfer band that was observed for **1** (Figure 1); however, the NMR spectral data of **2** are very similar to those of **1**. Specifically, its ^{1}H NMR spectrum in C_6D_6 features a singlet at 1.27 ppm, which is assignable to the 54 *tert*-butyl protons of the ketimide ligand, while multiplets at 6.67 and 7.00 ppm correspond to the *ortho* and overlapping *meta*/*para* phenyl protons of the ketimide ligand, respectively. In addition, the C=N resonance in the ^{13}C{^{1}H} NMR spectrum of **2** (178.73 ppm) is observed at a similar chemical shift to that of **1**. Lastly, its ^{7}Li{^{1}H} NMR spectra in C_6D_6 or toluene-d_8 feature single resonances at 0.53 and 0.47 ppm, respectively (Figures S10 and S12).

Interestingly, complex **2** also displays evidence of Li(N=C^{t}BuPh) dissociation in THF-d_8. Specifically, its ^{7}Li{^{1}H} NMR spectrum in this solvent features resonances at 1.90, 1.75, 0.61, and 0.04 ppm (Figure S14). The resonances at 1.90 and 1.75 ppm are assignable to Li(N=C^{t}BuPh), while the resonances at 0.61 and 0.04 ppm are assignable to **2** and [Li][Th(N=C^{t}BuPh$)_5$] (**2′**), respectively. These two Th complexes are present in a 1:5.5 ratio. As expected, addition of Li(N=C^{t}BuPh) to this sample results in an increase in the relative

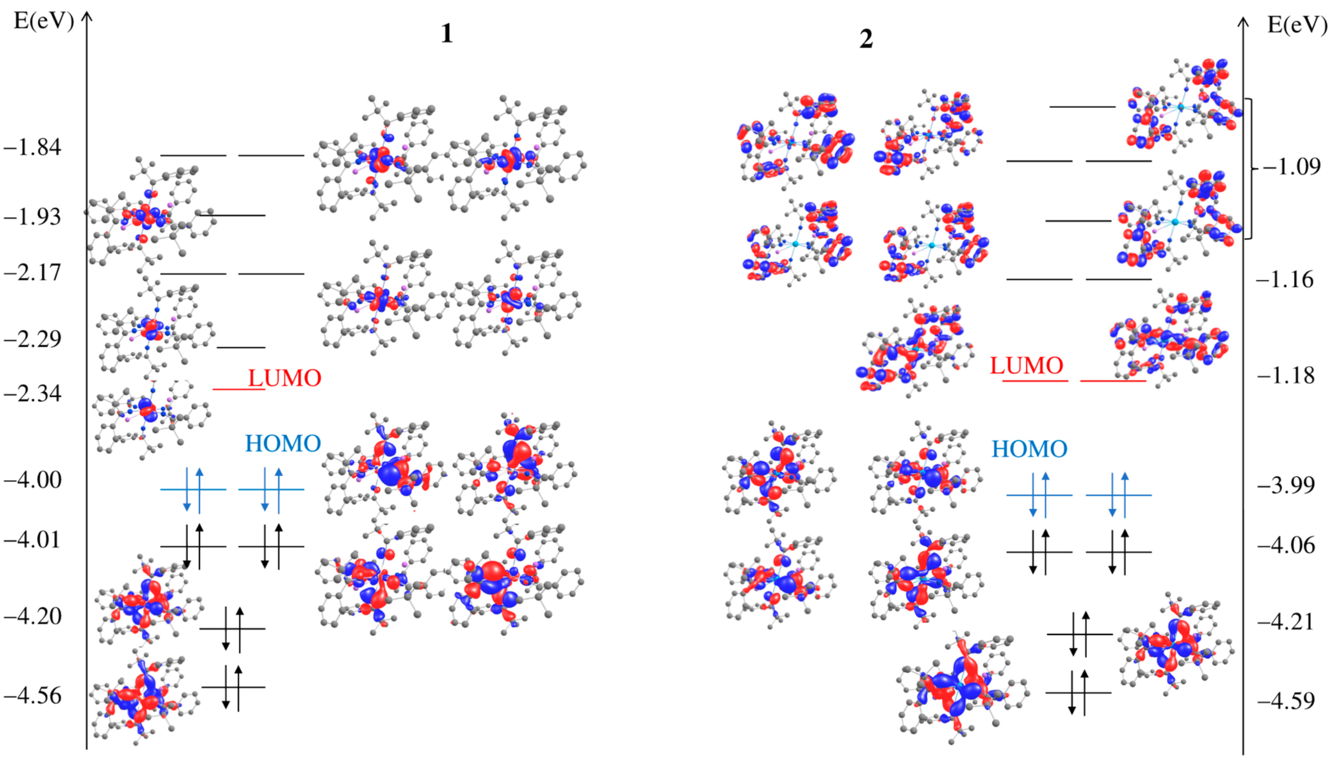

Figure 3. MO diagrams obtained with all-electron scalar relativistic DFT for **1** (left) and **2** (right). Canonical MO isosurfaces at ±0.03 au.

DOI: 10.1021/acs.inorgchem.9b01428
Inorg. Chem. XXXX, XXX, XXX−XXX

amount of **2**, and after addition of 8 equiv, **2** and **2′** are present in a 1:2 ratio (Figure S24). In contrast to the results collected for **2**, we see no evidence for the formation of **1** upon addition of excess Li(N=C^{t}BuPh) to THF-d_8 solutions of **1′** (Figure S20). This difference can be rationalized by the larger ionic radius of Th^{4+},[66] which allows this ion to better accommodate the high charge associated with six strongly donating ketimide ligands.

Storage of a concentrated toluene solution of **2** at −25 °C for 24 h afforded crystals suitable for X-ray analysis. As expected, complexes **1** and **2** are isostructural (Table S1). Additionally, the Th center in **2** possesses a distorted octahedral geometry (e.g., N1−Th1−N1* = 79.78(6)° and N1−Th1−N1** = 100.22(6)°). The Th−N distance (2.376(2) Å) is slightly longer than the Ce−N distance in **1** (2.338(5) Å) (Table 1) but is significantly longer than the U−N distance in the closely related U(V) ketimide [Li][U(N=C^{t}BuPh)$_6$] (2.217(2) Å),[55] in accord with their different ionic radii.[66] This distance is also considerably longer than those reported for the Th(IV) bis(ketimido) complex [Cp*$_2$Th(N=CPh$_2$)$_2$] (2.259(4) and 2.265(5) Å),[67] which may be due to the dianionic charge at the Th center, as well as the Li coordination to the ketimide N atoms. The lithium cations are hexa-coordinate and possess an octahedral geometry, with similar Li−N (2.166(4) Å) and Li−C_{ipso} (2.908(2) Å) distances to those observed for **1**. The C=N bond length (1.257(2) Å) is also identical to that in **1** (1.256(8) Å). Lastly, the Th−N−C angle in **2** (166.24(14)°) is essentially identical to the Ce−N−C angle in **1** (165.9(5)°), but it is more acute than the U−N−C angle in [Li][U(N=C^{t}BuPh)$_6$] (176.9(2)°).[55]

Computational Results. In an effort to understand the electronic structures of **1** and **2** and evaluate the possibility of a multiconfigurational ground state, a series of Kohn−Sham density functional calculations with the TPSS functional[68] and restricted/complete active space (RAS/CAS) self-consistent field[69] multiconfigurational wave function calculations were performed, using either the X-ray structural parameters of **1** and **2** or the $[M(N{=}CMe_2)_6]^{2-}$ (M = Ce, Th, Me = CH_3) truncated models (**t1**, **t2**) with C_i symmetry (Figure S35). Complete computational details are given in the Supporting Information. Figure 3 shows molecular orbital (MO) diagrams obtained for **1** and **2** with DFT. Both complexes exhibit frontier highest occupied MOs (HOMOs) with similar energetics, representing the six N-2p lone pairs exhibiting σ-donation to the metal centers. As **1** displays near-C_i symmetry and **2** obeys C_i symmetry, the six lone pairs form three gerade combinations that mix selectively with the metal valence 5d/6d orbitals and three ungerade combinations that mix selectively with the metal valence 4f/5f orbitals. The ligand−metal orbital mixing represents the donation bonding and is found to be stronger for **1** than for **2**. For instance, the Ce-4f contributions (weights) to the frontier HOMOs of **1** range from ∼7% to 12%, whereas the Th-5f contributions to the frontier HOMOs of **2** range from ∼3% to 5%.

The slightly more pronounced metal−ligand covalency in **1** versus **2** is also evidenced by the natural localized molecular orbitals (NLMOs) shown in Figure 4. According to the NLMO analyses, the Ce center in **1** is linked to the N atoms through nitrogen-polarized σ and π bonds, with ∼10% density weight at Ce. The σ-bonds employ mainly the 5d (58%) and 4f (28%) atomic orbitals (AOs) of Ce. The π-bonds have 53% 4f and 47% 5d AO contributions from Ce. The π-bonds are

1

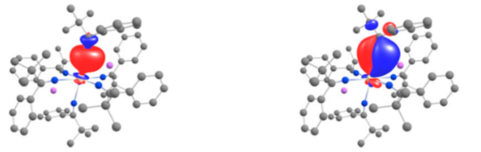

	σ(Ce–N)	π (Ce–N)
GTO/SDD	87% N (54 s; 46 p) 11% Ce (14 s; 58 d; 28 f)	81% N (100 p) 10% Ce (47 d; 53 f)
STO/ZORA	89% N (54 s; 46 p) 9% Ce (14 s; 59 d; 27 f)	83% N (100 p) 9% Ce (47 d; 53 f)

2

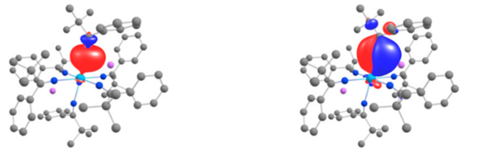

	σ(Th–N)	π (Th–N)
GTO/SDD	89% N (57 s; 43 p) 9% Th (17 s; 2 p; 58 d; 23 f)	84% N (100 p) 7% Th (1 s; 64 d; 35 f)
STO/ZORA	88% N (56 s; 44 p) 10% Th (13 s; 50 d; 37 f)	84% N (100 p) 8% Th (56 d; 44 f)

Figure 4. Bonding Ce−N (one σ and one π) natural localized molecular orbitals (isosurface of ±0.03 au) of **1** (top) and **2** (bottom), obtained with Gaussian-type orbital (GTO) vs Slater-type orbital (STO) basis sets. The π NLMO has slight five-center character; that is, there is a small delocalization tail toward adjacent C(butyl) and C(phenyl) centers. Weight percentages from Ce/Th and N centers are shown below the graphics. There are six equivalent such NLMO pairs corresponding to the six Ce−N interactions.

delocalized over the carbon end of the Ce−N−C units, as well as the adjacent C(butyl) and C(phenyl) centers, thus acquiring slight five-center character. The Ce 4f/5d character in the Ce−N bonds of **1** may explain its observed temperature-independent paramagnetism.[60] An important take-home message from the comparison of the NLMOs in **1** and **2** is that Ce engages with the 4f AOs more than Th does with the 5f AOs in both the σ and π NLMOs. Similar results were recently observed for series of isostructural cerium and thorium imido complexes.[70] Moreover, Ce(IV)−L bonds involving significant donation into the Ce-4f orbitals have been described previously.[27,45,71,72]

The same Ce−N bonding picture is predicted by all-electron relativistic calculations with the zeroth-order regular approximation (ZORA) Hamiltonian and by calculations where the relativistic valence-shell effects for the metal are introduced via a relativistic effective core potential (SDD), as demonstrated in Figure 4. Therefore, the absorption spectra of **1** and **2** can be modeled by calculations with the SDD core potentials, which are less demanding than the all-electron relativistic calculations. Before predicting the absorption spectrum with time-dependent DFT (TD-DFT), however, it is important to study the extent of multiconfigurational character of the ground state and, hence, the robustness of the single-configuration DFT calculations.

RAS and CAS wave function calculations were conducted on the C_i-symmetric **t1** and **t2** truncated model structures (Figure S35). These types of calculations were not feasible for **1** and **2** due to computational cost. **t1** and **t2** retain the same Ce coordination spheres and geometries as observed for **1** and **2**, as well as similar coordination environments for the C=N carbon atoms, and therefore the truncated models afford nearly

DOI: 10.1021/acs.inorgchem.9b01428
Inorg. Chem. XXXX, XXX, XXX−XXX

identical metal−ligand bonding as the parent structures. This is demonstrated explicitly by a comparison of the NLMOs of **1** and **t1** in Figures 4 and S36. The RAS calculations, using the N−C σ, π, σ^* and π^* (RAS1/3 subspaces) and the metal 4f/5f (RAS2) orbitals, determined ground states dominated by M(IV) (M = Ce or Th) closed-shell configurations for both **t1** and **t2** (86% weight). A similar outcome was reported for the multiply bonded Ce(IV) complex of ref 27. The RAS active space natural orbitals (NOs) and their occupancies (shown in Figure S37 for **t1**) show that the multiconfigurational character arises mainly from the N−C π-orbitals being correlated with their antibonding N−C π^* counterparts. Namely, the six N−C π orbitals have natural occupancies deviating from 2 (1.966 in **t1** and 1.949 in **t2**) and are the orbitals mainly responsible for the GS multiconfigurational character in the RAS calculations. CAS calculations for **t1** and **t2**, with only the N−C π and π^* orbitals taken as active, predicted a more pronounced multiconfigurational GS, with 77% weight for the M(IV) (M = Ce or Th) closed-shell configurations. The remaining weights correspond to intraligand N−C $\pi \rightarrow \pi^*$ doubly excited configurations. In the CAS calculations, the N−C π orbitals have natural occupancies deviating more strongly from 2 (1.918 for **t1** and 1.916 for **t2**) than in the RAS calculations. In view of the (TD-)DFT calculations, due to the approximations in the functional, the GS multiconfigurational character (static correlation) of **1** and **2** can be problematic, especially for the accurate prediction of the excited states involving the N−C/phenyl π^* orbitals. Accordingly, we performed the DFT and TD-DFT calculations with the TPSS meta-GGA functional,[68] because nonhybrid functionals are known to produce less-pronounced static correlation errors than their hybrid counterparts.[73]

The absorption spectra of **1** and **2**, calculated with TD-DFT/TPSS, are shown in Figure 5. With the chosen broadening parameters, the calculated and experimental spectra for both **1** and **2** agree very well, particularly in the 400−800 nm wavelength region, where the density of states is not very high. According to natural transition orbital (NTO) analyses, the electric dipole-intense transitions calculated above ca. 450 nm for **1**, giving rise to the distinct absorption peak, are generated by N-2p(lone pair) → Ce-4f charge transfer excited states (Figure S38). Dipole-intense transitions calculated for **1** below 450 nm are generally generated by N-2p(lone pair) → N−C (π^*)/phenyl (π^*) charge transfer. The calculated absorption spectrum for **2** shows comparable intensity to the spectrum of **1** only below 450 nm, in agreement with the experiments. According to NTO analyses of the electric dipole-intense transitions (Figure S39), the absorption intensity of **2** is generated by intraligand N-2p(lone pair) → N−C (π^*)/phenyl (π^*) charge transfer, as it is the case for **1** in the same wavelength region.

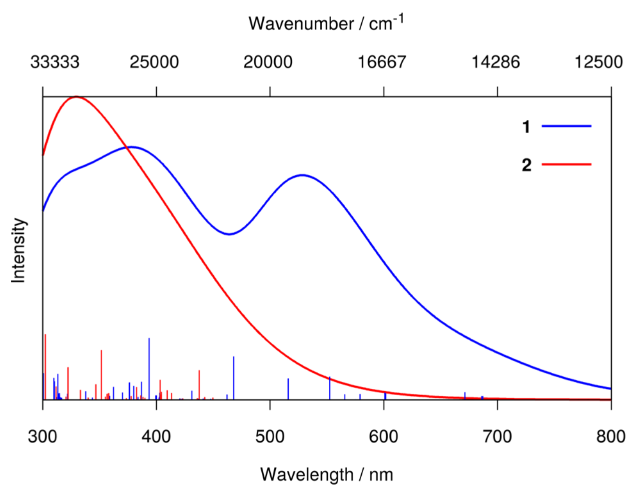

Figure 5. TD-DFT/TPSS UV−vis spectra of **1** and **2** calculated with a solvent model for toluene. The spectra were obtained with a 3000/7000 cm^{-1} Gaussian broadening of the calculated transitions for the 12 500−20 000/20 000−35 000 cm^{-1} energy ranges. The "stick spectra" represent calculated oscillator strengths. For **1**, the spectral features above 450 nm are due to N-2p(lone pair) → Ce(4f) transitions, whereas the spectral features below 450 nm are due to N-2p(lone pair) → phenyl (π^*)/C−N (π^*) transitions. For **2**, spectral features appear below 450 nm due to N-2p(lone pair) → phenyl (π^*)/C−N (π^*) transitions. NTO analyses are shown in Figures S38 and S39.

Most importantly, the TD-DFT calculations agree with the experiments with respect to the presence/absence of a long wavelength ligand-to-metal charge transfer band in the absorption spectrum of **1**/**2**. The observation can be readily explained based on the MO diagrams shown in Figure 3. In the case of **1**, the formally nonbonding Ce-4f orbitals are represented by the weakly antibonding metal-centered lowest unoccupied molecular orbital (LUMO) to LUMO+6. These are the first MOs available for the electronic transitions. In contrast, for **2** the low-energy unoccupied MOs consist of mixed N−C (π^*)/phenyl (π^*) MOs, while the Th-5f orbitals appear at much higher energy. The energy gap between the occupied N-2p (lone pair) combinations and the Ce-4f orbitals in **1** versus the N−C (π^*)/phenyl (π^*) LUMOs in **2** (see Figure 3) is 2.10 eV (590 nm) and 3.10 eV (400 nm), respectively, matching well with the intensity onsets in the calculated and measured absorption spectra.

Cyclic Voltammetry. To better understand the donor ability of the ketimide ligand, we investigated the electrochemical properties of **1** and **2** by cyclic voltammetry. The cyclic voltammogram of **1** in THF at a scan rate of 200 mV/s exhibits an irreversible redox feature at $E_{p,c}$ = −2.16 V (vs Fc/Fc$^+$, Figure 6), which we attribute to the Ce(IV/III) reduction of [Li][Ce(N═C^{t}BuPh)$_5$] (**1′**). This feature remains irreversible, even at scan rates of 2000 mV/s. Our assignment was confirmed by comparison with the cyclic voltammogram recorded for complex **2**, which features no reduction features

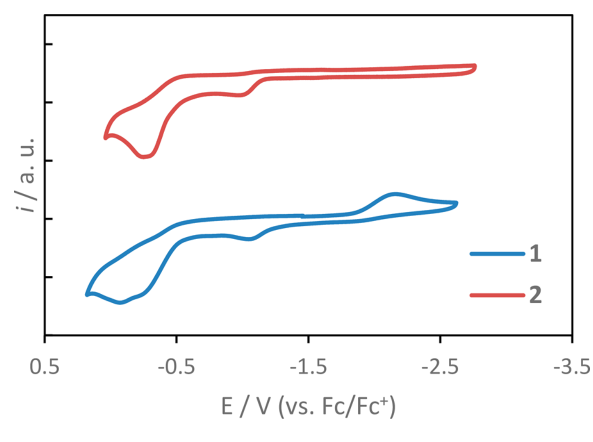

Figure 6. Cyclic voltammograms of **1** and **2** (200 mV/s scan rate, vs Fc/Fc$^+$). Measured in THF with 0.1 M [NBu$_4$][BPh$_4$] as the supporting electrolyte.

DOI: 10.1021/acs.inorgchem.9b01428
Inorg. Chem. XXXX, XXX, XXX−XXX

within the solvent window (Figure 6). The cyclic voltammograms of **1** and **2** also exhibit a complex series of irreversible oxidation features between −1.1 and 0 V (vs Fc/Fc^+), which we attribute to ligand oxidation events. Similar ligand-based oxidation features were observed in the cyclic voltammogram of the related uranium ketimide, $[U(N{=}C^tBuPh)_6]$,[55] as well as for $Li(N{=}C^tBuPh)$ (Figure S30).

The Ce(IV/III) redox feature observed for **1′** is among the lowest reported for this element (Table 2). For comparison,

Table 2. Ce(IV/III) Redox Potentials for Selected Cerium Complexes

complex	potential[a] (V)	conditions[b]
$[Ce(acac)_4]$[58]	0.22 ± 0.02 vs SHE	0.1 M $TBAPF_6$ in MeCN/acetone
$[CeL]^{4-}$,[29]	−0.454 vs SHE	1 M KCl
$[Li_3][(binolate)_3Ce]$[43]	−1.09 vs Fc/Fc^+	0.1 M TPAB in THF
$[Ce(BIPM^{TMS})_2]$[46]	−1.63 V	0.1 M TPAB in THF
$[Ce(omtaa)_2]$[41]	−1.7 vs Fc/Fc^+	0.1 M TPAB in THF
$[Ce(OSi(O^tBu)_3)_4]$[44]	−1.72 vs Fc/Fc^+	0.1 M $[NBu_4][B(C_6F_5)_4]$ in THF
$\{Ce(atrane)(OAr)\}_2$[16]	−1.86 vs Fc/Fc^+	0.1 M TPAB in THF
$[Ce(pyNO)_4]$[9]	−1.95 vs Fc/Fc^+	0.1 M TPAB in DCM
$[Ce(L')(O^tBu)_2]$[42]	−2.07 vs Fc/Fc^+	0.5 M TPAB in THF
1′	−2.16 vs Fc/Fc^+	0.1 M $TBABPh_4$ in THF
$[Ce(L'')(O^tBu)_2]$[42]	−2.39 vs Fc/Fc^+	0.5 M TPAB in THF
$[Ce(NP(pip)_3)_4]$[14]	−2.30 to −2.47 vs Fc/Fc^+	
$[Ce(NP(pip)_3)_4]^-$[14]	−2.64 to −3.10 vs Fc/Fc^+	

[a]SHE = standard hydrogen electrode. [b]TPAB = $[^nPr_4N][B(3,5\text{-}(CF_3)_2C_6H_3)_4]$, $TBAPF_6$ = $[NBu_4][PF_6]$, $TBABPh_4$ = $[NBu_4][BPh_4]$.

the cerium(III) tris(binolate) complex $[Li(THF)]_3[(binolate)_3Ce(THF)]$ features an electrochemically irreversible Ce(IV/III) reduction feature at −1.09 V (vs Fc/Fc^+),[43,74] which is much more anodic than that observed for **1′**, suggesting that the ketimide ligand better stabilizes the Ce(IV) oxidation state than the binolate ligand. For further comparison, the Ce(IV/III) reduction features for the ferrocene-bridged Schiff base complexes $[Ce(L')(O^tBu)_2]$ ($L'H_2$ = 1,1′-di(2,4-bis-*tert*-butyl-salicylimino)ferrocene) and $[Ce(L'')(O^tBu)_2]$ ($L''H_2$ = 1,1′-di(2-*tert*-butyl-salicyl-(bis-phenyl)-iminophosphorano)ferrocene) are at −2.07 and −2.39 V (vs Fc/Fc^+), respectively.[42] These values are more in-line with the redox potential observed for **1′**. Similarly, the Ce(IV/III) reduction potential for $[Ce(NP(pip)_3)_4]$ in THF was recently determined to be within the range from −2.30 to −2.47 V (vs Fc/Fc^+).[14]

■ SUMMARY

We have prepared and structurally characterized the homoleptic cerium ketimide $[Li]_2[Ce(N{=}C^tBuPh)_6]$ (**1**), along with its thorium analogue $[Li]_2[Th(N{=}C^tBuPh)_6]$ (**2**). DFT calculations on **1** and **2** reveal the presence of polarized σ and π Ce/Th−N bonding interactions with modest metal−ligand covalency, which is somewhat larger for **1** than for **2**. RAS/CAS self-consistent field calculations suggest moderate multiconfigurational character for the ground states dictated by intraligand electron correlation, mainly among the N−C π and π^* orbitals. The ground state of **1** and **2** is dominated by the M(IV) closed-shell configuration in the wave function calculations (86/77% with RAS/CAS). Moreover, DFT calculations show that, for **1**, the Ce-4f orbitals are represented by the lowest-energy unoccupied MOs, which are responsible for a unique long-wavelength absorption band that is not seen for **2**. Finally, an electrochemical analysis of **1** revealed one of the most cathodic Ce(IV)/Ce(III) reduction potentials yet recorded, due, in part, to the strongly donating nature of the ketimide ligand along with the anionic charge at the Ce center, and indicating considerable stabilization of the Ce(IV) state. Our electrochemical results suggest that, for cerium at least, the ketimide ligand is more strongly donating than alkoxide but less donating than phosphiniminato. Going forward, we will examine the ability of the ketimide ligand to stabilize Pr^{4+} and Tb^{4+}. This goal seems all the more plausible given the recent isolation and crystallographic characterization of two Tb^{4+} complexes.[44,75]

■ ASSOCIATED CONTENT

Supporting Information

The Supporting Information is available free of charge on the ACS Publications website at DOI: 10.1021/acs.inorgchem.9b01428.

Experimental, crystallographic, and computational details for complexes **1** and **2** (PDF)

Accession Codes

CCDC 1916136−1916137 contain the supplementary crystallographic data for this paper. These data can be obtained free of charge via www.ccdc.cam.ac.uk/data_request/cif, or by emailing data_request@ccdc.cam.ac.uk, or by contacting The Cambridge Crystallographic Data Centre, 12 Union Road, Cambridge CB2 1EZ, UK; fax: +44 1223 336033.

■ AUTHOR INFORMATION

Corresponding Authors

*E-mail: jochena@buffalo.edu. (J.A.)
*E-mail: hayton@chem.ucsb.edu. (T.W.H.)

ORCID

Dumitru-Claudiu Sergentu: 0000-0001-6570-5245
Jochen Autschbach: 0000-0001-9392-877X
Trevor W. Hayton: 0000-0003-4370-1424

Notes

The authors declare no competing financial interest.

■ ACKNOWLEDGMENTS

We thank the National Science Foundation (CHE 1764345) for financial support of this work. This research made use of the 400 MHz NMR spectrometer of the UCSB Chemistry Department, an NIH SIG (1S10OD012077-01A1). The MRL Shared Experimental Facilities are supported by the MRSEC Program of the National Science Foundation under Award No. NSF DMR 1720256; a member of the NSF-funded Materials Research Facilities Network. D.-C.S and J.A. acknowledge support from the U.S. Department of Energy, Office of Basic Energy Sciences, Heavy Element Chemistry program, Grant No. DE-SC0001136, for the theory component of this study, and the Center for Computational Research (CCR, http://hdl.handle.net/10477/79221) at the Univ. at Buffalo for providing computational resources. We also thank J. D. Bocarsly for helpful discussions about our magnetism data.

DOI: 10.1021/acs.inorgchem.9b01428
Inorg. Chem. XXXX, XXX, XXX−XXX

■ REFERENCES

(1) Anwander, R.; Dolg, M.; Edelmann, F. T. The difficult search for organocerium(iv) compounds. *Chem. Soc. Rev.* **2017**, *46*, 6697−6709.
(2) Avignant, D.; Largeau, E.; Gaumet, V.; Dugat, P.; El-Ghozzi, M. Recent progress in tetravalent terbium chemistry. *J. Alloys Compd.* **1998**, *275−277*, 1−5.
(3) El-Ghozzi, M.; Avignant, D. Crystal chemistry and magnetic structures of Tb(IV) fluorides. *J. Fluorine Chem.* **2001**, *107*, 229−233.
(4) Hobart, D. E.; Young, J. P.; Norvell, V. E.; Mamantov, G.; Peterson, J. R.; Samhoun, K. Stabilization of praseodymium(IV) and terbium(IV) in aqueous carbonate solution. *Inorg. Nucl. Chem. Lett.* **1980**, *16*, 321−328.
(5) Sroor, F. M.; Edelmann, F. T. Lanthanides: Tetravalent Organometallic. *In Encycl. Inorg. Bioinorg. Chem.* Scott, R. A., Ed., 2012, 1−14.
(6) Eller, P. G.; Penneman, R. A. Stabilization of actinides and lanthanides in high oxidation states. *J. Less-Common Met.* **1987**, *127*, 19−33.
(7) Nugent, L. J.; Baybarz, R. D.; Burnett, J. L.; Ryan, J. L. Electron-transfer and f-d absorption bands of some lanthanide and actinide complexes and the standard (II-III) oxidation potential for each member of the lanthanide and actinide series. *J. Phys. Chem.* **1973**, *77*, 1528−1539.
(8) Beckers, J.; Rothenberg, G. Sustainable selective oxidations using ceria-based materials. *Green Chem.* **2010**, *12*, 939−948.
(9) Bogart, J. A.; Lewis, A. J.; Medling, S. A.; Piro, N. A.; Carroll, P. J.; Booth, C. H.; Schelter, E. J. Homoleptic Cerium(III) and Cerium(IV) Nitroxide Complexes: Significant Stabilization of the 4+ Oxidation State. *Inorg. Chem.* **2013**, *52*, 11600−11607.
(10) Gorte, R. J. Ceria in catalysis: From automotive applications to the water-gas shift reaction. *AIChE J.* **2010**, *56*, 1126−1135.
(11) Lammert, M.; Wharmby, M. T.; Smolders, S.; Bueken, B.; Lieb, A.; Lomachenko, K. A.; Vos, D. D.; Stock, N. Cerium-based metal organic frameworks with UiO-66 architecture: synthesis, properties and redox catalytic activity. *Chem. Commun.* **2015**, *51*, 12578−12581.
(12) Levin, J. R.; Dorfner, W. L.; Dai, A. X.; Carroll, P. J.; Schelter, E. J. Density Functional Theory as a Predictive Tool for Cerium Redox Properties in Nonaqueous Solvents. *Inorg. Chem.* **2016**, *55*, 12651−12659.
(13) Piro, N. A.; Robinson, J. R.; Walsh, P. J.; Schelter, E. J. The electrochemical behavior of cerium(III/IV) complexes: Thermodynamics, kinetics and applications in synthesis. *Coord. Chem. Rev.* **2014**, *260*, 21−36.
(14) Rice, N. T.; Su, J.; Gompa, T. P.; Russo, D. R.; Telser, J.; Palatinus, L.; Bacsa, J.; Yang, P.; Batista, E. R.; La Pierre, H. S. Homoleptic Imidophosphorane Stabilization of Tetravalent Cerium. *Inorg. Chem.* **2019**, *58*, 5289−5304.
(15) So, Y.-M.; Leung, W.-H. Recent advances in the coordination chemistry of cerium(IV) complexes. *Coord. Chem. Rev.* **2017**, *340*, 172−197.
(16) Solola, L. A.; Cheisson, T.; Yang, Q.; Carroll, P. J.; Schelter, E. J. Exploration of the Solid- and Solution-State Structures and Electrochemical Properties of Ce^{IV}(atrane) Complexes. *Inorg. Chem.* **2018**, *57*, 10543−10547.
(17) Das, A. K. Kinetic and mechanistic aspects of metal ion catalysis in cerium(IV) oxidation. *Coord. Chem. Rev.* **2001**, *213*, 307−325.
(18) Molander, G. A. Application of lanthanide reagents in organic synthesis. *Chem. Rev.* **1992**, *92*, 29−68.
(19) Nair, V.; Balagopal, L.; Rajan, R.; Mathew, J. Recent Advances in Synthetic Transformations Mediated by Cerium(IV) Ammonium Nitrate. *Acc. Chem. Res.* **2004**, *37*, 21−30.
(20) Nair, V.; Deepthi, A. Cerium(IV) Ammonium Nitrate - A Versatile Single-Electron Oxidant. *Chem. Rev.* **2007**, *107*, 1862−1891.
(21) Sridharan, V.; Menéndez, J. C. Cerium(IV) Ammonium Nitrate as a Catalyst in Organic Synthesis. *Chem. Rev.* **2010**, *110*, 3805−3849.
(22) Binnemans, K. Applications of tetravalent cerium compounds. In *Handbook on the Physics and Chemistry of Rare Earths;* Gschneidner, K. A., Bunzli, J.-C. G., Pecharsky, V. K., Eds.; Elsevier, 2006; Vol. *36*; pp 281−392.
(23) Ellis, R. J.; Antonio, M. R. Redox Chemistry of Third Phases Formed in the Cerium/Nitric Acid/Malonamide-n-Dodecane Solvent Extraction System. *ChemPlusChem* **2012**, *77*, 41−47.
(24) Berryman, V. E. J.; Whalley, Z. J.; Shephard, J. J.; Ochiai, T.; Price, A. N.; Arnold, P. L.; Parsons, S.; Kaltsoyannis, N. Computational analysis of M-O covalency in $M(OC_6H_5)_4$ (M = Ti, Zr, Hf, Ce, Th, U). *Dalton Trans* **2019**, *48*, 2939−2947.
(25) Bianconi, A.; Marcelli, A.; Tomellini, M.; Davoli, I. Determination of mixing of 4f-ligand orbitals in $Ce(SO_4)_2$ by XANES. Is $Ce(SO_4)_2$ a mixed valent insulating system? *J. Magn. Magn. Mater.* **1985**, *47−48*, 209−211.
(26) Clark, D. L.; Gordon, J. C.; Hay, P. J.; Poli, R. Existence and Stability of Lanthanide−Main Group Element Multiple Bonds. New Paradigms in the Bonding of the 4f Elements. A DFT Study of Cp_2CeZ (Z = F^+, O, NH, CH^-, CH_2) and the Ligand Adduct $Cp_2Ce(CH_2)(NH_3)$. *Organometallics* **2005**, *24*, 5747−5758.
(27) Gregson, M.; Lu, E.; Tuna, F.; McInnes, E. J. L.; Hennig, C.; Scheinost, A. C.; McMaster, J.; Lewis, W.; Blake, A. J.; Kerridge, A.; Liddle, S. T. Emergence of comparable covalency in isostructural cerium(iv)- and uranium(iv)-carbon multiple bonds. *Chem. Sci.* **2016**, *7*, 3286−3297.
(28) Minasian, S. G.; Batista, E. R.; Booth, C. H.; Clark, D. L.; Keith, J. M.; Kozimor, S. A.; Lukens, W. W.; Martin, R. L.; Shuh, D. K.; Stieber, S. C. E.; Tylisczcak, T.; Wen, X.-d. Quantitative Evidence for Lanthanide-Oxygen Orbital Mixing in CeO_2, PrO_2, and TbO_2. *J. Am. Chem. Soc.* **2017**, *139*, 18052−18064.
(29) Pham, T. A.; Altman, A. B.; Stieber, S. C. E.; Booth, C. H.; Kozimor, S. A.; Lukens, W. W.; Olive, D. T.; Tyliszczak, T.; Wang, J.; Minasian, S. G.; Raymond, K. N. A Macrocyclic Chelator That Selectively Binds Ln^{4+} over Ln^{3+} by a Factor of 10^{29}. *Inorg. Chem.* **2016**, *55*, 9989−10002.
(30) Ashley, A.; Balazs, G.; Cowley, A.; Green, J.; Booth, C. H.; O'Hare, D. Bis(permethylpentalene)cerium - another ambiguity in lanthanide oxidation state. *Chem. Commun.* **2007**, 1515−1517.
(31) Halbach, R. L.; Nocton, G.; Booth, C. H.; Maron, L.; Andersen, R. A. Cerium Tetrakis(tropolonate) and Cerium Tetrakis(acetylacetonate) Are Not Diamagnetic but Temperature-Independent Paramagnets. *Inorg. Chem.* **2018**, *57*, 7290−7298.
(32) Isago, H.; Shimoda, M. Mixed Valence State of Cerium in Bis(phthalocyaninato)cerium Complex. *Chem. Lett.* **1992**, *21*, 147−150.
(33) Mooßen, O.; Dolg, M. Assigning the Cerium Oxidation State for CH_2CeF_2 and $OCeF_2$ Based on Multireference Wave Function Analysis. *J. Phys. Chem. A* **2016**, *120*, 3966−3974.
(34) Streitwieser, A.; Kinsley, S. A.; Jenson, C. H.; Rigsbee, J. T. Synthesis and Properties of Di-π-[8]annulenecerium(IV), Cerocene. *Organometallics* **2004**, *23*, 5169−5175.
(35) Booth, C. H.; Walter, M. D.; Daniel, M.; Lukens, W. W.; Andersen, R. A. Self-Contained Kondo Effect in Single Molecules. *Phys. Rev. Lett.* **2005**, *95*, 267202.
(36) Mooßen, O.; Dolg, M. Two interpretations of the cerocene electronic ground state. *Chem. Phys. Lett.* **2014**, *594*, 47−50.
(37) Walter, M. D.; Booth, C. H.; Lukens, W. W.; Andersen, R. A. Cerocene Revisited: The Electronic Structure of and Interconversion Between $Ce_2(C_8H_8)_3$ and $Ce(C_8H_8)_2$. *Organometallics* **2009**, *28*, 698−707.
(38) Löble, M. W.; Keith, J. M.; Altman, A. B.; Stieber, S. C. E.; Batista, E. R.; Boland, K. S.; Conradson, S. D.; Clark, D. L.; Lezama Pacheco, J.; Kozimor, S. A.; Martin, R. L.; Minasian, S. G.; Olson, A. C.; Scott, B. L.; Shuh, D. K.; Tyliszczak, T.; Wilkerson, M. P.; Zehnder, R. A. Covalency in Lanthanides. An X-ray Absorption Spectroscopy and Density Functional Theory Study of $LnCl_6^{x-}$ (x = 3, 2). *J. Am. Chem. Soc.* **2015**, *137*, 2506−2523.
(39) Aneggi, E.; Boaro, M.; Leitenburg, C. d.; Dolcetti, G.; Trovarelli, A. Insights into the redox properties of ceria-based oxides and their implications in catalysis. *J. Alloys Compd.* **2006**, *408−412*, 1096−1102.
(40) Vivier, L.; Duprez, D. Ceria-Based Solid Catalysts for Organic Chemistry. *ChemSusChem* **2010**, *3*, 654−678.

DOI: 10.1021/acs.inorgchem.9b01428
Inorg. Chem. XXXX, XXX, XXX−XXX

(41) Williams, U. J.; Mahoney, B. D.; Lewis, A. J.; DeGregorio, P. T.; Carroll, P. J.; Schelter, E. J. Single Crystal to Single Crystal Transformation and Hydrogen-Atom Transfer upon Oxidation of a Cerium Coordination Compound. *Inorg. Chem.* **2013**, *52*, 4142−4144.
(42) Broderick, E. M.; Thuy-Boun, P. S.; Guo, N.; Vogel, C. S.; Sutter, J.; Miller, J. T.; Meyer, K.; Diaconescu, P. L. Synthesis and Characterization of Cerium and Yttrium Alkoxide Complexes Supported by Ferrocene-Based Chelating Ligands. *Inorg. Chem.* **2011**, *50*, 2870−2877.
(43) Robinson, J. R.; Carroll, P. J.; Walsh, P. J.; Schelter, E. J. The Impact of Ligand Reorganization on Cerium(III) Oxidation Chemistry. *Angew. Chem., Int. Ed.* **2012**, *51*, 10159−10163.
(44) Palumbo, C. T.; Zivkovic, I.; Scopelliti, R.; Mazzanti, M. Molecular Complex of Tb in the + 4 Oxidation State. *J. Am. Chem. Soc.* **2019**, *141*, 9827−9831.
(45) Gregson, M.; Lu, E.; McMaster, J.; Lewis, W.; Blake, A. J.; Liddle, S. T. A Cerium(IV)-Carbon Multiple Bond. *Angew. Chem., Int. Ed.* **2013**, *52*, 13016−13019.
(46) Gregson, M.; Lu, E.; Mills, D. P.; Tuna, F.; McInnes, E. J. L.; Hennig, C.; Scheinost, A. C.; McMaster, J.; Lewis, W.; Blake, A. J.; Kerridge, A.; Liddle, S. T. The inverse-trans-influence in tetravalent lanthanide and actinide bis(carbene) complexes. *Nat. Commun.* **2017**, *8*, 14137.
(47) Damon, P. L.; Liss, C. J.; Lewis, R. A.; Morochnik, S.; Szpunar, D. E.; Telser, J.; Hayton, T. W. Quantifying the Electron Donor and Acceptor Abilities of the Ketimide Ligands in $M(N{=}C^tBu_2)_4$ (M = V, Nb, Ta). *Inorg. Chem.* **2015**, *54*, 10081−10095.
(48) Lewis, R. A.; George, S. P.; Chapovetsky, A.; Wu, G.; Figueroa, J. S.; Hayton, T. W. Synthesis of a cobalt(iv) ketimide with a squashed tetrahedral geometry. *Chem. Commun.* **2013**, *49*, 2888−2890.
(49) Lewis, R. A.; Wu, G.; Hayton, T. W. Synthesis and Characterization of an Iron(IV) Ketimide Complex. *J. Am. Chem. Soc.* **2010**, *132*, 12814−12816.
(50) Lewis, R. A.; Wu, G.; Hayton, T. W. Stabilizing High-Valent Metal Ions with a Ketimide Ligand Set: Synthesis of $Mn(N{=}C^tBu_2)_4$. *Inorg. Chem.* **2011**, *50*, 4660−4668.
(51) Soriaga, R. A. D.; Nguyen, J. M.; Albright, T. A.; Hoffman, D. M. Diamagnetic Group 6 Tetrakis(di-tert-butylketimido)metal(IV) Complexes. *J. Am. Chem. Soc.* **2010**, *132*, 18014−18016.
(52) Lewis, R. A.; Smiles, D. E.; Darmon, J. M.; Stieber, S. C. E.; Wu, G.; Hayton, T. W. Reactivity and Mössbauer Spectroscopic Characterization of an Fe(IV) Ketimide Complex and Reinvestigation of an Fe(IV) Norbornyl Complex. *Inorg. Chem.* **2013**, *52*, 8218−8227.
(53) Graves, C. R.; Vaughn, A. E.; Schelter, E. J.; Scott, B. L.; Thompson, J. D.; Morris, D. E.; Kiplinger, J. L. Probing the Chemistry, Electronic Structure and Redox Energetics in Organometallic Pentavalent Uranium Complexes. *Inorg. Chem.* **2008**, *47*, 11879−11891.
(54) Kiplinger, J. L.; Morris, D. E.; Scott, B. L.; Burns, C. J. The First f-Element Ketimido Complex: Synthesis and Characterization of $(C_5Me_5)_2U(=NCPh_2)_2$. *Organometallics* **2002**, *21*, 3073−3075.
(55) Seaman, L. A.; Wu, G.; Edelstein, N.; Lukens, W. W.; Magnani, N.; Hayton, T. W. Probing the 5f Orbital Contribution to the Bonding in a U(V) Ketimide Complex. *J. Am. Chem. Soc.* **2012**, *134*, 4931−4940.
(56) Damon, P. L.; Wu, G.; Kaltsoyannis, N.; Hayton, T. W. Formation of a Ce(IV) Oxo Complex via Inner Sphere Nitrate Reduction. *J. Am. Chem. Soc.* **2016**, *138*, 12743−12746.
(57) The observation of two resonances for $Li(N{=}C^tBuPh)$ can be explained by invoking the presence of lithium ketimide clusters with different nuclearities. See: Reed, D.; Barr, D.; Mulvey, R. E.; Snaith, R. High-field lithium-7 nuclear magnetic resonance spectroscopic and cryoscopic relative molecular mass studies on solutions of amido- and imido-lithium compounds. *J. Chem. Soc., Dalton Trans.* **1986**, 557−564.
(58) Behrsing, T.; Bond, A. M.; Deacon, G. B.; Forsyth, C. M.; Forsyth, M.; Kamble, K. J.; Skelton, B. W.; White, A. H. Cerium acetylacetonates—new aspects, including the lamellar clathrate $[Ce(acac)_4]\cdot 10H_2O$. *Inorg. Chim. Acta* **2003**, *352*, 229−237.
(59) Walter, M. D.; Fandos, R.; Andersen, R. A. Synthesis and magnetic properties of cerium macrocyclic complexes with tetramethyldibenzotetraaza[14]annulene, $tmtaaH_2$. *New J. Chem.* **2006**, *30*, 1065−1070.
(60) Eisenstein, J. C.; Pryce, M. H. L. The electronic structure and magnetic properties of uranyl-like ions I. Uranyl and neptunyl. *Proc. R. Soc. London. Ser. A* **1955**, *229*, 20−38.
(61) Fowler, P. W.; Steiner, E. Temperature-independent paramagnetism in closed-shell oxanions of first-row transition metals. *J. Chem. Soc., Faraday Trans.* **1993**, *89*, 1915−1924.
(62) Mullane, K. C.; Hrobárik, P.; Cheisson, T.; Manor, B. C.; Carroll, P. J.; Schelter, E. J. ^{13}C NMR Shifts as an Indicator of U-C Bond Covalency in Uranium(VI) Acetylide Complexes: An Experimental and Computational Study. *Inorg. Chem.* **2019**, *58*, 4152−4163.
(63) Schneider, D.; Spallek, T.; Maichle-Mossmer, C.; Tornroos, K. W.; Anwander, R. Cerium tetrakis(diisopropylamide) - a useful precursor for cerium(iv) chemistry. *Chem. Commun.* **2014**, *50*, 14763−14766.
(64) Hitchcock, P. B.; Lappert, M. F.; Protchenko, A. V. Facile formation of a homoleptic Ce(iv) amide via aerobic oxidation. *Chem. Commun.* **2006**, 3546−3548.
(65) Crozier, A. R.; Bienfait, A. M.; Maichle-Mössmer, C.; Törnroos, K. W.; Anwander, R. A homoleptic tetravalent cerium silylamide. *Chem. Commun.* **2013**, *49*, 87−89.
(66) Shannon, R. D. Revised effective ionic radii and systematic studies of interatomic distances in halides and chalcogenides. *Acta Crystallogr., Sect. A: Cryst. Phys., Diffr., Theor. Gen. Crystallogr.* **1976**, *32*, 751−767.
(67) Jantunen, K. C.; Burns, C. J.; Castro-Rodriguez, I.; Da Re, R. E.; Golden, J. T.; Morris, D. E.; Scott, B. L.; Taw, F. L.; Kiplinger, J. L. Thorium(IV) and Uranium(IV) Ketimide Complexes Prepared by Nitrile Insertion into Actinide−Alkyl and −Aryl Bonds. *Organometallics* **2004**, *23*, 4682−4692.
(68) Tao, J.; Perdew, J. P.; Staroverov, V. N.; Scuseria, G. E. Climbing the Density Functional Ladder: Nonempirical Meta−Generalized Gradient Approximation Designed for Molecules and Solids. *Phys. Rev. Lett.* **2003**, *91*, 146401.
(69) Malmqvist, P. A.; Rendell, A.; Roos, B. O. The restricted active space self-consistent-field method, implemented with a split graph unitary group approach. *J. Phys. Chem.* **1990**, *94*, 5477−5482.
(70) Cheisson, T.; Kersey, K. D.; Mahieu, N.; McSkimming, A.; Gau, M. R.; Carroll, P. J.; Schelter, E. J. Multiple Bonding in Lanthanides and Actinides: Direct Comparison of Covalency in Thorium(IV)- and Cerium(IV)-Imido Complexes. *J. Am. Chem. Soc.* **2019**, *141*, 9185−9190.
(71) Duignan, T. J.; Autschbach, J. Impact of the Kohn-Sham Delocalization Error on the 4f Shell Localization and Population in Lanthanide Complexes. *J. Chem. Theory Comput.* **2016**, *12*, 3109−3121.
(72) Qiao, Y.; Sergentu, D.-C.; Yin, H.; Zabula, A. V.; Cheisson, T.; McSkimming, A.; Manor, B. C.; Carroll, P. J.; Anna, J. M.; Autschbach, J.; Schelter, E. J. Understanding and Controlling the Emission Brightness and Color of Molecular Cerium Luminophores. *J. Am. Chem. Soc.* **2018**, *140*, 4588−4595.
(73) Cohen, A. J.; Mori-Sánchez, P.; Yang, W. Challenges for Density Functional Theory. *Chem. Rev.* **2012**, *112*, 289−320.
(74) Robinson, J. R.; Gordon, Z.; Booth, C. H.; Carroll, P. J.; Walsh, P. J.; Schelter, E. J. Tuning Reactivity and Electronic Properties through Ligand Reorganization within a Cerium Heterobimetallic Framework. *J. Am. Chem. Soc.* **2013**, *135*, 19016−19024.
(75) Rice, N. T.; Popov, I. A.; Russo, D. R.; Bacsa, J.; Batista, E. R.; Yang, P.; Telser, J.; La Pierre, H. S. Design, Isolation, and Spectroscopic Analysis of a Tetravalent Terbium Complex. *J. Am. Chem. Soc.* **2019**, *141*, 13222−13233.

DOI: 10.1021/acs.inorgchem.9b01428
Inorg. Chem. XXXX, XXX, XXX−XXX